http://eprints.gla.ac.uk/83368/

Deposited on: 16 September 2013

Enhanced Fano resonance of organic material films deposited on arrays of asymmetric split-ring resonators (A-SRRs)

Basudev Lahiri,[1,3] Scott G. McMeekin,[2,*] Richard M. De La Rue,[1] and Nigel P. Johnson[1]

[1]School of Engineering, University of Glasgow, Glasgow G12 8LT, UK
[2]School of Engineering and Built Environment, Glasgow Caledonian University, Glasgow, G4 0BA, UK
[3]Present address: NIST, Center for Nanoscale Science and Technology, Gaithersburg, MD 20899, USA
[*]scott.mcmeekin@gcu.ac.uk

Abstract: Depositing very thin organic films on the surface of arrays of asymmetric split-ring resonators (A-SRRs) produces a shift in their resonance spectra that can be utilized for sensitive analyte detection. Here we show that when poly-methyl-methacrylate (PMMA) is used as an organic probe (analyte) on top of the A-SRR array, the phase and amplitude of a characteristic molecular Fano resonance associated with a carbonyl bond changes according to the spectral positions of the trapped mode resonance of the A-SRRs and their plasmonic reflection peaks. Furthermore, we localize blocks of PMMA at different locations on the A-SRR array to determine the effectiveness of detection of very small amounts of non-uniformly distributed analyte.

References and links

1. C. Debus and P. H. Bolivar, "Frequency selective surfaces for high sensitivity terahertz sensing," Appl. Phys. Lett. **91**(18), 184102 (2007).
2. P. H. Bolivar, M. Nagel, M. Richter, M. Brucherseifer, H. Kruz, A. Bosserhoff, and R. Buttner, "Label-free THz sensing of genetic sequences towards 'THZ biochips'," Philos. Trans. R. Soc. Lond. A **362**(1815), 323–335 (2004).
3. V. A. Fedotov, M. Rose, S. L. Prosvirnin, N. Papasimakis, and N. I. Zheludev, "Sharp trapped-mode resonances in planar metamaterials with a broken structural symmetry," Phys. Rev. Lett. **99**(14), 147401 (2007).
4. M. S. Rill, C. Plet, M. Thiel, I. Staude, G. von Freymann, S. Linden, and M. Wegener, "Photonic metamaterials by direct laser writing and silver chemical vapour deposition," Nat. Mater. **7**(7), 543–546 (2008).
5. M. Brucherseifer, M. Nagel, P. H. Bolivar, H. Kurz, A. Basserhoff, and R. Buttner, "Label-free probing of the binding state of DNA by time-domain terahertz sensing," Appl. Phys. Lett. **77**(24), 4049–4051 (2000).
6. J. Aizpurua, T. Taubner, F. J. García de Abajo, M. Brehm, and R. Hillenbrand, "Substrate-enhanced infrared near-field spectroscopy," Opt. Express **16**(3), 1529–1545 (2008).
7. J. F. Federici, B. Schulkin, F. Huang, D. Gary, R. Barat, F. Oliveira, and D. Zimdars, "THz imaging and sensing for security applications — explosives, weapons and drugs," Semicond. Sci. Technol. **20**(7), S266–S280 (2005).
8. B. Lahiri, A. Z. Khokhar, R. M. De La Rue, S. G. McMeekin, and N. P. Johnson, "Asymmetric split ring resonators for optical sensing of organic materials," Opt. Express **17**(2), 1107–1115 (2009).
9. P. Ding, E. J. Liang, W. Q. Hu, G. W. Cai, and Q. Z. Xue, "Tunable plasmonic properties and giant field enhancement in asymmetric double split ring arrays," Photon. Nanostructures **9**(1), 42–48 (2011).
10. E. Cubukcu, S. Zhang, Y-S. Park, G. Bartal, and X. Zhang, "Split ring resonator sensors for infrared detection of single molecular monolayers," Appl. Phys. Lett. **95**, 043113 (2009).
11. C. Wu, A. B. Khanikaev, R. Adato, N. Arju, A. A. Yanik, H. Altug, and G. Shvets, "Fano-resonant asymmetric metamaterials for ultrasensitive spectroscopy and identification of molecular monolayers," Nat. Mater. **11**(1), 69–75 (2011).
12. I. M. Pryce, K. Aydin, Y. Kelaita, R. M. Briggs, and H. A. Atwater, "Compliant metamaterials for resonantly enhanced infrared absorption spectroscopy and refractive index sensing," ACS Nano. **5**, 8167–8174 (2011).
13. B. Lahiri, S. G. McMeekin, R. M. De La Rue, and N. P. Johnson, "Resonance hybridization in nanoantenna arrays based on asymmetric split-ring resonators," Appl. Phys. Lett. **98**, 153116 (2011).
14. D. H. Williams and I. Fleming, "Spectroscopic methods in organic chemistry," (McGraw Hill Publication, 1973) 2nd Edition. Chapter 2.

15. A. Balamurugan, S. Kannan, V. Selvaraj, and S. Rajeswari, "Development and spectral characterization of Poly(Methyl Methacrylate) /Hydroxyapatite composite for biomedical applications," Trends Biomaterials Artif Organs. **18**, 41–45 (2004).
16. L. H. Lee and W. C. Chen, "High refractive index thin films prepared from Trialkoxysilane-capped Poly(methyl methacrylate)-Titania hybrid materials," Chem. Mater. **13**(3), 1137–1142 (2001).
17. P. S. Nunes, N. A. Mortensen, J. P. Kutter, and K. B. Mogensen, "Photonic crystal resonator integrated in a microfluidic system," Opt. Lett. **33**, 1623–1625 (2008).
18. A. Soldera and E. Monterrat, "Mid-infrared optical properties of a polymer film: comparison between classical molecular simulations, spectrometry, and ellipsometry techniques," Polymer (Guildf.) **43**(22), 6027–6035 (2002).

1. Introduction

Optical sensing and identification of thin-film organic substances are the subject of much current research activity due to their large potential for commercial application [1–3]. It is possible to identify an organic substance by detecting the characteristic phonon absorption resonances of the molecular compound from its complex dielectric properties, using various optical methods [1–7]. Sensitive and accurate detection of minute amounts of organic compounds is required for a number of purposes such as forensic and security analyses - and immuno-sensing [7]. Arrays of asymmetric split-ring resonators (A-SRRs) with resonant features in the infrared spectral region can exhibit significantly modified responses when there is a change in the overall dielectric environment [1,8]. The modification of the resonant response of A-SRRs is a sensitive function of the characteristics and the amount of added dielectric material - and hence may be utilized for detection of small quantities of the material.

By using A-SRR nano-antenna arrays that resonate in the infrared region of the electromagnetic spectrum, a number of advantages are obtained. Firstly, the asymmetry in the A-SRR type split-ring resonators produces characteristically steeper responses than those obtained by their symmetric counterparts. The trapped mode resonance produces a lower value of reflectance between the two reflectance maxima [9] - and hence potentially greater sensitivity to the presence of a deposited thin film or partial thin film [8].

Secondly, by matching the responses of A-SRRs with the targeted molecular resonance of the organic compound, the characteristic signature of that molecule is obtained [8]. Even minute amounts of organic materials can be detected when they are non-uniformly distributed to specific positions on the A-SRR nano-antenna array. As described in our previous work [8] the resonant frequency of A-SRRs scales inversely with size [1–3,8] - and the nano-antenna arrays of A-SRRs with circular geometry act as passive frequency selective surfaces (FSSs) at infrared frequencies. Later work by Cubukcu et al. [10], and Wu et al. [11] has also shown detection of molecular resonances in somewhat similar structures and materials - and similar results have been obtained in mechanically tunable structures by Pryce et al. [12]. In this paper we show: (a) how the combined resonance of the molecular probe and the A-SRR resonators can be modeled as Fano (Lorentz) resonance behavior determined by the organic molecular properties, (b) how the effect on the phase and amplitude of the molecular Fano-resonance varies with the spectral position in relation to the spectral response of the A-SRRs, and (c) the relative sensitivity of the observed resonance spectral position to the localized spatial position of the organic molecular probe region.
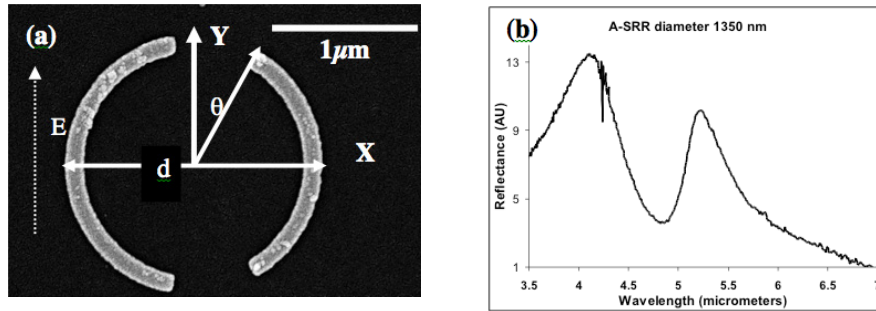
Fig. 1. Asymmetric split ring resonator (A-SRR) and its subsequent reflectance spectra: (a) Single A-SRR SEM micrograph, showing the orientation of the E-field parallel to the Y axis. (b) Measurements at normal incidence) showing corresponding reflectance spectra. The crest at 4.07 μm wavelength is the resonance of the smaller arc (right-hand). The crest at a wavelength of 5.21 μm is the resonance primarily of the large (left-hand) arc. The trough at 4.81 μm is the trapped mode.

A-SRRs were fabricated in thin gold films on fused silica substrates, using a combination of electron-beam lithography (EBL) and lift-off processing. After EBL patterning of bi-layer PMMA resist, 2 nm of titanium and then 48 nm of gold were deposited, followed by lift-off. Square array patterns were written over areas of 300 μm x 300 μm. The reflection spectra of the fabricated structures were measured at normal incidence with a Nicolet Continuum FTIR apparatus equipped with an optical microscope. The FTIR beam was polarized using a Continuum ZnSe IR polarizer. Reflectance measurements were normalized, after each measurement, to the reflectivity of a gold coated mirror. Simulations were carried out using Lumerical FDTD Solutions software to determine the reflection spectra of the A-SRR structures and the distribution of the electric field components induced in the A-SRR structures by the incident infrared radiation.

Figure 1(a) shows the scanning electron microscope (SEM) image of one such unit cell of a fabricated A-SRR nano-antenna array. It involves two opposite and distinct arcs separated by equal angular gaps (θ). The two arcs of the A-SRR (left hand and right hand) act separately as reflection resonators, each having their own individual response. The reflection response of each arc depends on its length, as well as the angular gap (θ) between the two arcs. In each case the measurement is taken at normal incidence (i.e. the Z-direction), with the exciting electric field maintained parallel to the Y direction.

When A-SRRs are illuminated at normal incidence with linearly polarized light, the electric field of the incident plane wave excites current in both of the constituent arcs, with the resonant reflection frequency of each arc being determined inversely by its length. For A-SRRs the individual resonances of the arcs are distinct, because of the difference in their lengths – but, due to the proximity of the two arcs, their reflection resonances are coupled and modified by their mutual presence [13]. In addition, a trapped resonant mode can be excited in which current circulates around both arcs of the combined A-SRR structure. This trapped-mode situation reduces the coupling of the resonant mode to free space, and therefore decreases the radiation losses [3,8,13]. A substantial increase in the absorption takes place, corresponding to a minimum in both the reflectance and transmittance spectra – and this situation is consistent with the energy being stored and dissipated in the coupled arcs [3,8,13]. Figure 1(b) shows the corresponding reflectance spectra (measured) from an array made of nearly ten thousand A-SRRs.

Many organic compounds contain molecular bonds that exhibit spectral resonances in the mid-infrared range (typically in the 3-6 μm wavelength range) [14]. This property has provided the main motivation, in our work, for tuning the resonant response of the A-SRRs to mid infrared wavelengths. In order to test the sensitivity of the A-SRRs, the fabricated

structures were coated with thin films of poly-methyl-methacrylate (PMMA), a commonly used positive electron-beam resist. PMMA was chosen because it has a well-defined spectral resonance in the mid infra-red wavelength region and accurate control of the thickness is obtainable via the spin speed used when coating the sample. The use of PMMA as a probe material for modifying the plasmonic behavior has been described in a previous reference [6]. PMMA exhibits a strong spectral resonance at a wavelength of about 5.8 µm. This feature is due to the $C = O$ stretching band of unconjugated ester, i.e. the free carbonyl bond [15,16] - and it is the strongest feature observable when taking FTIR spectra of thin films of PMMA deposited over fused silica substrates. PMMA also displays other, relatively weaker molecular resonances at shorter wavelengths around 3.4 µm, due to stretching of CH_2 and CH_3 bonds, and at longer wavelengths around 6.63 µm, due to bending of CH3 bonds [15,16].

By changing the diameter of the A-SRRs it is possible to match the various resonances of the arcs to the molecular resonance of the carbonyl bond of PMMA, which results in the formation of sharpened spectral features and enhancement of the sensitivity.

2. A-SRR resonances modified by the presence of a thin organic film

Figure 2 indicates close agreement between measurements and simulations of the A-SRR nano-antenna array, with and without the PMMA film. The results show that the resonances have been shifted to longer wavelengths by the addition of the PMMA film and the molecular resonance of the carbonyl bond is clearly visible at 5.8 µm. For A-SRRs with a diameter of 1.35 µm, Fig. 2(a), the peak of the longer wavelength resonance (for the left-hand arc) matches that of the molecular vibration resonance of the carbonyl bond resonance of PMMA. When the diameter of the A-SRRs is changed to 1.55 µm, Fig. 2(b), the trapped mode of the A-SRRs matches the carbonyl bond resonance. A further increase in the diameter of the A-SRR to 1.70 µm, Fig. 2(c), results in a close match between the shorter wavelength resonance and the carbonyl bond resonance.

3. Sensitivity to the presence of thin organic films

The sensitivity, s, of the reflection properties of the array of A-SRRs to the presence of deposited PMMA may be expressed as [17]:

$$s = \frac{\Delta \lambda}{\Delta n} \, nm \, / \, RIU . \qquad (1)$$

where $\Delta \lambda$ is the shift in resonance wavelength and Δn is the change in the overall refractive index. The sensitivity, s, is often quoted in nanometers (nm) per Refractive Index Unit (RIU).

From Fig. 2(b) it can be seen that a 100 nm thick PMMA layer shifts the longer resonance peak wavelength of the A-SRR by 600 nm - from 5.8 µm to 6.4 µm. The PMMA layer covers the entire 50 nm thick A-SRR nano-antenna array and replaces the air above the A-SRR, so the change in refractive index is obtained as $\Delta n = 1.49 - 1 = 0.49$.

Therefore, the sensitivity of the A-SRR for a 100 nm thick PMMA layer becomes

$$s = \frac{600}{1.49 - 1} = 1230 \, nm \, / \, RIU . \qquad (2)$$
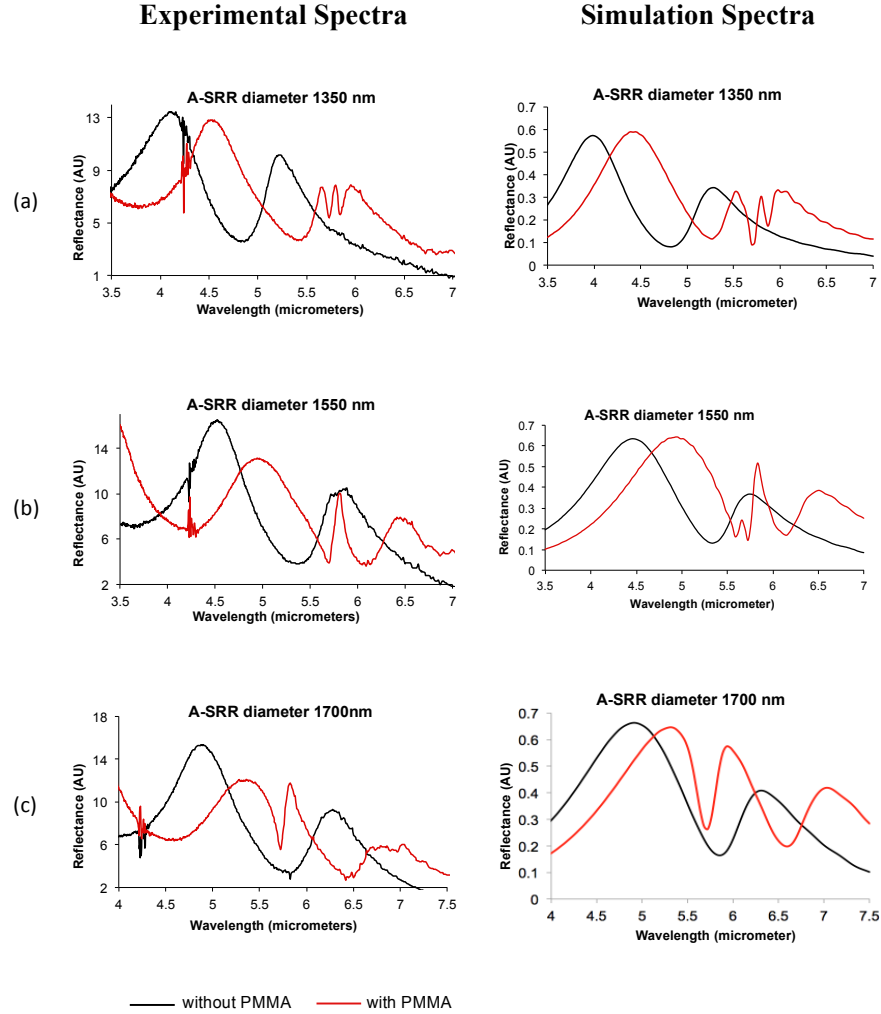
Experimental Spectra

Simulation Spectra

Fig. 2. Table depicting the shift in the position of the resonance produced by tuning the size of the A-SRRs and loading them with a 110 nm thick layer of PMMA. Black curves depict the original A-SRR reflectance, while red curves denote the shift in the spectra due to loading of PMMA. The second column depicts the corresponding simulations. The spike present at a wavelength of 4.2 μm in all the experimental spectra indicates the presence of atmospheric carbon dioxide.

4. Enhancement of the molecular resonance of the thin organic film

The PMMA layer was modeled as a Lorentz oscillator material in which the background relative permittivity of the PMMA layer modifies the standard Lorentz resonance to produce a Fano type resonance defined by:

$$\varepsilon(f) = \varepsilon + \frac{\varepsilon_{Lorentz}\,\omega_o^2}{\left(\omega_o^2 - 2i\,\delta_o\,\omega - \omega^2\right)}. \tag{3}$$

where ω_o is the Lorentz resonance frequency of 3.269 x 10^{14} rad.s^{-1} and ε is the background relative permittivity of PMMA, 2.2. The values of the Lorentz permittivity, $\varepsilon_{Lorentz}$, of 0.04 and the Lorentz linewidth, δ_o, of 8.0x 10^{11} rad.s^{-1} have been selected to provide a close match with the experimental measurements.

The Fano type resonance associated with the PMMA molecules (essentially formed by the Lorentz resonance superimposed on a slowly varying dielectric back ground) produces both negative and positive changes in the refractive index of the PMMA layer, as well as a strongly frequency dependent absorption coefficient. Figure 3 shows the value of the refractive index and the absorption coefficient of PMMA given by the Fano type resonance defined in Eq. (3).
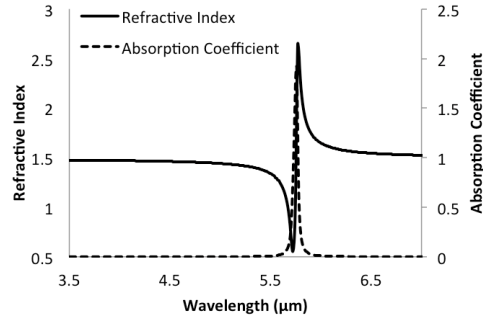

Fig. 3. Refractive index and absorption coefficient of PMMA with a Fano type resonance of the carbonyl bond at 5.8 microns.

The Fano type resonance in the refractive index of the PMMA layer at 5.8 μm will result in a shift in the reflectance spectra of the A-SRR array at this specific wavelength. As the wavelength of the incident light approaches the carbonyl bond resonance the refractive index of the PMMA decreases rapidly. This results in a shift of the reflectance spectra of the A-SRR array to shorter wavelengths. At the resonant wavelength of the carbonyl bond the refractive index of the PMMA film flips to a sudden increase in value. This results in a shift in the reflectance spectra of the A-SRR array to longer wavelengths.

The resultant shape of the reflection spectra can be regarded as a spectrally localized shift of the A-SRR resonance(s) within the line-width of the Fano resonance that is proportional to the change in the refractive index.

In Fig. 2(a), the carbonyl bond resonance coincides with the peak in the resonance spectrum of the longer wavelength A-SRR resonance - and the spectrally localized shift in the plasmonic resonance induced by the Fano resonance results in multiple peaks and dips in the reflectance amplitude. Figure 2(b) shows a large single peak corresponding to an increase in the reflectance as the position of the trapped mode is shifted by the presence of the thin film of dielectric material. Figure 2(c) shows a large single dip in the reflectance spectrum as the position of the shorter wavelength resonance is shifted by the Fano resonance.

5. Sensitivity to localized organic analyte

To further test the effectiveness of the A-SRR nano-antenna arrays for sensing, small blocks of PMMA were localized at different points with respect to the elements of the array, in order to assess the sensitivity of A-SRR nano-antenna arrays to detect analyte that is non-uniformly distributed over the sensing surface. The approach used builds on our initial demonstration of the Lorentz resonance from PMMA interacting with the A-SRR resonance in addition to the local index change.

In order to localize PMMA at specific positions of the A-SRR nano-antenna array, a two-step registration alignment technique is followed. First, markers are defined using electron-beam exposure and developed and then subjected to an electron-beam deposition of 50 nm nichrome and 150 nm of gold, followed by lift-off. After the markers are defined in this way, the substrate is coated with resist and again subjected to another set of electron-beam exposure processes for aligning and defining the A-SRR structures between the markers. After development, a further electron-beam deposition of 2 nm of titanium and 48 nm of gold,

followed by another lift-off process is required. After the A-SRRs are clearly defined within the markers, a thin layer of PMMA of thickness around 100 nm is deposited - and is then again subjected to selective e-beam exposure, followed by development to localize the PMMA at specific positions on the A-SRR arrays. At the end of the process, square blocks of PMMA with an area of ~200 nm x 200 nm - and thickness 100 nm - remain at specific positions with respect to the elements of the A-SRR array.
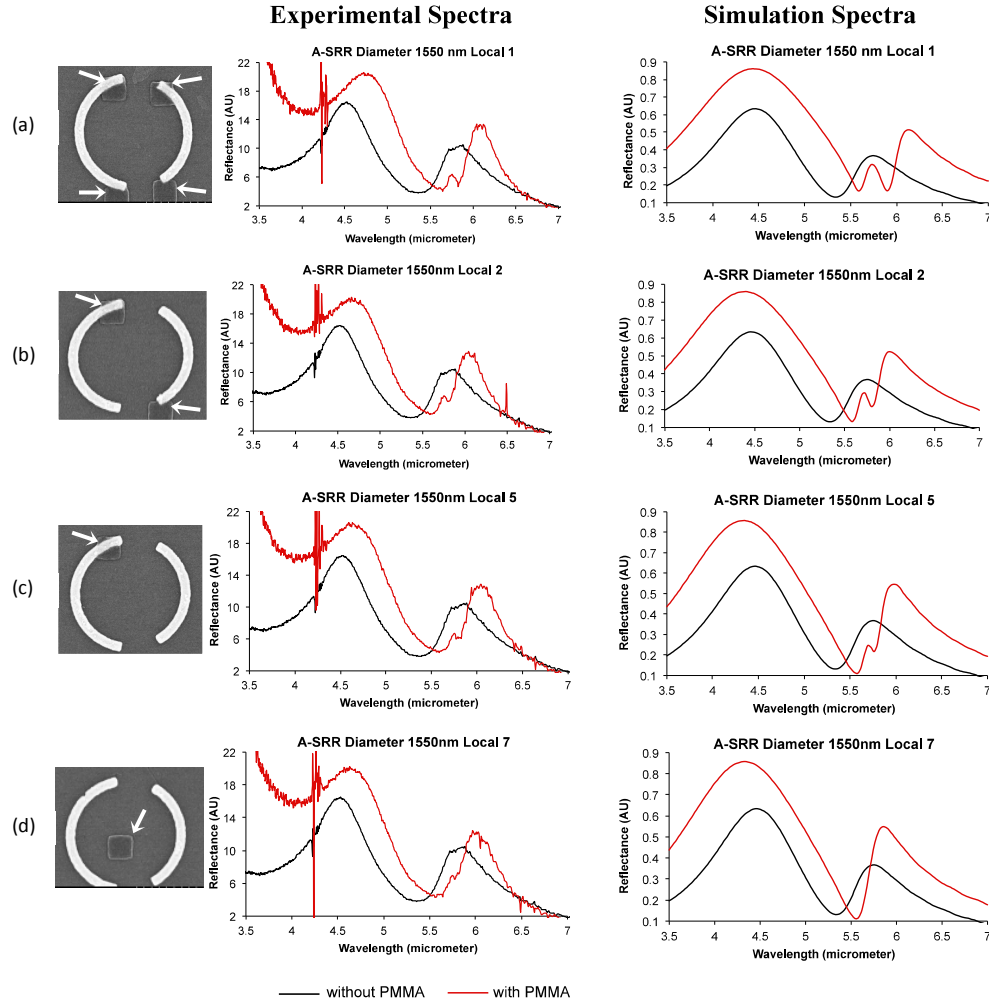

Fig. 4. Table depicting the shift in the position of the resonance produced by A-SRRs of diameter 1550 nm when loaded with localized PMMA: (a) Four PMMA blocks at each end of A- SRR arms (b) Two PMMA blocks at diagonally opposite A-SRR arms (c) One PMMA block at only one arm of the A-SRR (d) One PMMA block at the middle of the A-SRR. The first column shows the SEM images with the localized PMMA blocks identified by the white arrows. The second column with solid lines shows the experimental reflectance spectra. Black curves show the original A-SRR reflectance, red curves denotes the shift in the spectra due to loading of localized PMMA. The third column.shows the corresponding simulations.

Figure 4 shows the SEM images of localized PMMA at different positions of the A-SRR, along with their corresponding reflectance spectra. In Fig. 4 the experimental and simulation spectra are in good agreement with one another. It can be seen in Fig. 4 that the reflection spectrum of the A-SRR nano-antenna array undergoes a substantial shift from the original

spectrum when loaded with blocks of PMMA in specific locations – and there is a significant relative enhancement of the molecular resonance.

In the case of Fig. 4(a), the overall volume of PMMA in the array is approximately 60 times less than in the film for which results are shown in Fig. 2. Yet, the A-SRR array is able to give a sensitivity of 636 nm/RIU, experimentally. Clearly the shift is dependent on the amount of material present in the A-SRR nano-antenna array and, moreover, on its position with respect to the arcs and gaps of the A-SRRs. In the case of Figs. 4(c) and 4(d), the overall volume of PMMA is approximately 240 times less than in the previous experiments of Fig. 2, and yet it shows a sensitivity of 346 nm/RIU, experimentally.

Along with the distinct shift in the overall spectra, the A-SRR is also capable of highlighting and enhancing the strong Fano type resonance of the carbonyl bond of the PMMA at 5.8 µm. As the amount of analyte reduces, as shown in Figs. 4(a)-4(c), the detected signal reduces. A comparison of the carbonyl bond resonance between Figs. 4(c) and 4(d) shows that the sensitivity of the array is much higher when the analyte is close to the ends of the metallic arcs of the A-SRRs.

The discrepancies between simulation and experiment in the results shown in Fig. 4 may be explained by the limitations of Lorentz model used to define the PMMA in the simulations and by the influence of the PMMA on the resonance hybridization produced by the interaction between the arcs [13]. The Lorentz model defined in Eq. (3) is limited to a single resonance to describe the carbonyl bond and does not include the other molecular resonances that are present in PMMA [18]. The increase at the extreme left of the experiment spectra may be explained by the C-H resonance around 3.4 µm, which is not present in the simulation results. The impact of the C-H resonance may be enhanced by higher order plasmonic resonances of the A-SRR elements.

Resonance hybridization, due to the coupling between the arcs in the A-SRR, produces a red shift of both peaks as described in [13], The magnitude of the red shift will be dependent on the proximity of the resonant peaks to each other. In Figs. 4(b)–4(d) the location of the PMMA block will result in a larger red shift for the long wavelength peak than the short wavelength peak. This will increase the difference between the peak wavelengths and result in a weakening of the red shift produced by resonance hybridization. This behavior is observed in Figs. 4(c) and 4(d), which both show a blue shift in the short wavelength peak due to the weaker resonance hybridization while the long wavelength peak is red shifted due to the presence of PMMA. The lack of blue shift in the experimental results may be attributed to the proximity of the C-H resonance.

In addition, the actual locations of the PMMA squares in the fabricated samples are not the ideal ones assumed in the simulations. This observation is most clearly evident in the row of Fig. 4(d), where the PMMA square in the fabricated sample is not located in the exact center of the defining circles of the A-SRR, as is assumed for the simulation. The simulation therefore shows no indication at all, of the molecular Fano resonance feature, whereas it is clearly but weakly visible in the experimental result.

Figure 5 shows the computed magnitude of the electric field component perpendicular to the surface of the substrate, Ez, induced in the A-SRR structure at the resonant wavelength of the carbonyl bond. It can be seen from Fig. 5 that the maximum magnitude of the electric field component Ez induced in the A-SRR structure is located at the end of the arcs. When the sample of analyte is located on or adjacent to the end of an arc, the relatively stronger electric fields of the infra-red electromagnetic wave couple with the analyte and enhance the molecular resonance. The enhanced resonance corresponds to the peak in the reflectance spectra at 5.8 µm shown in Fig. 4. The different intensities of the electric field shown in Fig. 5(a) and 5(b) are due to the perturbation of the resonance of the trapped mode by the localized PMMA. In comparison: in Fig. 5(d), where the analyte is localized in the center of the A-SRR, there is very weak coupling between the electric field and the PMMA, which corresponds to a reduction in the peak reflectance spectrum at 5.8 µm, as shown in Fig. 4(d).

It should also be noted that the field concentration effect, when a PMMA block is present, clearly can occur at either end of both the longer arm and the shorter arm of each A-SRR, with the parameters chosen.
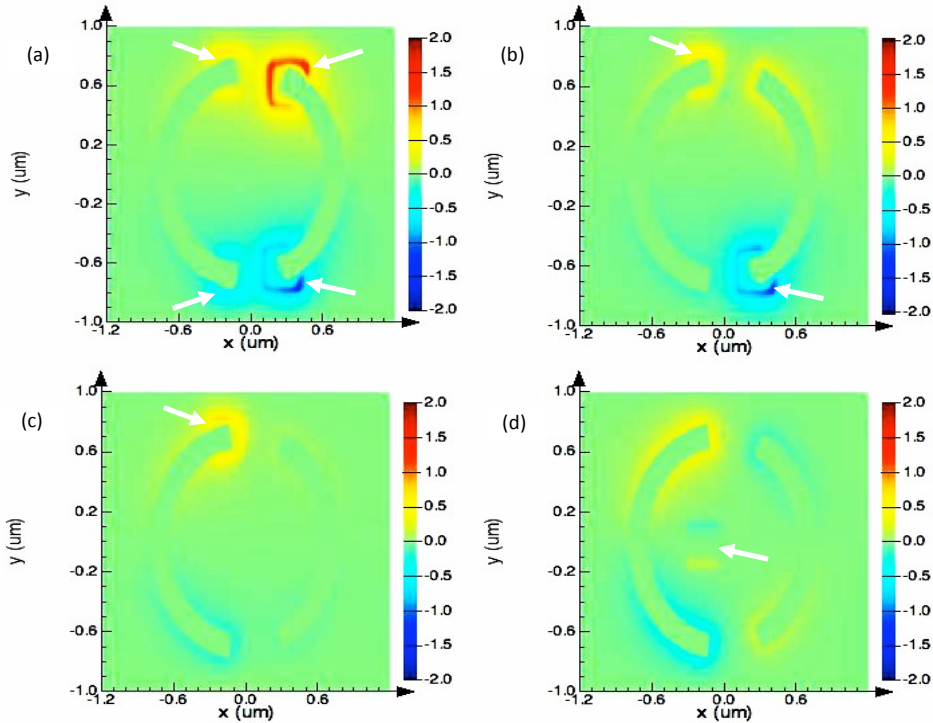

Fig. 5. Intensity plots of the induced electric field (in Arbitrary Units) normal to the plane, Ez, at the PMMA resonant wavelength, 5.8 microns. The localized blocks of PMMA are identified by white arrows. (a) Four PMMA blocks at the end of A-SRR arms (b) Two PMMA blocks at diagonally opposite A-SRR arms (c) One PMMA block at only one arm of the A-SRR (d) One PMMA block at the middle of the A-SRR.

6. Conclusions

In summary, the operation of the A-SRR nano-antenna array has been described and utilized for the detection of very thin PMMA films. A Fano (Lorentz) model accurately describes the spectra of the combined A-SRR molecular resonances. The negative-positive oscillation of the refractive index of the molecular (Fano) resonance coupled with the slope of the shifted A-SRR peaks gives rise to the different line shapes that are observed experimentally and are closely matched by the simulations. Furthermore, small PMMA regions have been localized at different positions on the A-SRR elements – in addition to covering the whole array, in order to demonstrate the strong position dependence of the relative sensitivity.

From an identification viewpoint, it may be desirable to operate either with A-SRRs that are tuned so that the molecular resonance coincides with one of the two peak reflection regions of the A-SRRs - or with the molecular resonance coinciding with the trapped mode region between the reflection peaks. The choice between these situations will possibly be determined by the engineering of specific instrumentation for maximum sensitivity. Real organic materials, of which PMMA is simply one specific polymeric example, will quite typically have several different molecular bond vibration resonance features. The use of separate arrays of A-SRRs with different dimensions should make it possible to make identification a more complete process and enable distinction to be made between similar but different molecules.

Acknowledgments